PHYSICAL REVIEW C **76**, 065204 (2007)

Spectral functions of scalar mesons

Francesco Giacosa and Giuseppe Pagliara
Institut für Theoretische Physik, Universität Frankfurt, Johann Wolfgang Goethe Universität, Max von Laue Str. 1, D-60438 Frankfurt, Germany
(Received 24 July 2007; published 10 December 2007)

In this work we study the spectral functions of scalar mesons in one- and two-channel cases by using nonlocal interaction Lagrangian(s). When the propagators satisfy the Källen-Lehman representation, a normalized spectral function is obtained, allowing one to take into account finite-width effects in the evaluation of decay rates. In the one-channel case, suitable to the light σ and k mesons, the spectral function can deviate consistently from a Breit-Wigner shape. In the two-channel case with one subthreshold channel, the evaluated spectral function is well approximated by a Flatté distribution; when applying the study to the $a_0(980)$ and $f_0(980)$ mesons, the tree-level forbidden KK decay is analyzed.

DOI: 10.1103/PhysRevC.76.065204 PACS number(s): 14.40.Cs, 12.39.Mk

I. INTRODUCTION

The scalar mesons below 2 GeV have been a center of debate for many years [1–4]. More states than expected from the quark-antiquark assignment are reported in Particle Data Group (PDG) [5], leading to the introduction of a scalar glueball [6], tetraquark states [7], and mesonic molecules [8]. In particular, the scalar resonances below 1 GeV have appealing characteristics, such as the reversed level ordering of masses, expected from tetraquark states [3,7,9–11]. In turn, this scenario implies that quarkonia lie between 1 and 2 GeV. A complication in the analysis of scalar states is mixing: between 1 and 2 GeV a quarkonia-glueball mixing in the isoscalar sector is considered, for instance, in Ref. [12]. Mixing among tetraquark states below 1 GeV and quarkonia above 2 GeV is studied in Refs. [13–15], where, however, the results do not coincide: while a large mixing is found in Ref. [14], a negligible mixing is the outcome of Ref. [15]. It should be stressed that different interpretations of scalar state are possible: a nonet of scalar quarkonia is settled below 1 GeV in Ref. [16] in agreement with the linear σ model and the Nambu Jona-Lasinio (NJL) model, while in Ref. [17] a broad glueball, to be identified with $f_0(600)$, is proposed. We refer the reader to Refs. [1–3,10] for a discussion of arguments in favor of and against the outlined assignments.

Studies on scalar mesons have been extensively performed by using chiral perturbation theory [18], where a scalar resonance at about 440 MeV is inferred out of pion-pion scattering. A full nonet of molecularlike scalar states is generated in the unitarized chiral perturbation theory of Ref. [19]. In particular, Pelaez [20] studied the large-N_c dependence of the light scalar resonances, finding that they do not scale as quarkonia but agree with a molecular or tetraquark composition (see, however, also the discussions in Ref. [21]).

In the present paper, we concentrate on an important aspect of light scalar resonances, namely, the form of their spectral functions, in a simple theoretical context. In this study, relevant to both quarkonium and tetraquark assignment of light scalars [22], effects arising from loops of pseudoscalar mesons are considered: this leads to parametrizations of spectral functions beyond the (usually employed) Breit-Wigner and Flatté distributions and allow us to include finite-width effects in the evaluation of decay rates. In particular, we consider the following physical scenarios: (i) the case of a broad scalar resonance, strongly coupled to one decay channel, such as the $\sigma \equiv f_0(600)$ in the pion-pion decay mode, for which the spectral function can deviate substantially from the Breit-Wigner form; (ii) the case of two channels, one of which is subthreshold for the mass and thus forbidden at the tree level, as the $\overline{K}K$ decay mode for the resonances $f_0(980)$ and $a_0(980)$. In the latter case, a comparison with the usually employed Flatté distribution is performed.

A crucial aspect of our study is to consider a nonlocal interaction Lagrangian, which implies a ultraviolet regularization and directly affects the real and imaginary part of the mesonic loop. In a phenomenological perspective, it is reasonable that the mesonic states in the loop cannot have indefinitely high virtual momenta which are naturally limited due to the finite range of the meson-meson interaction. We also show that the dependence on the chosen cutoff function, specifying the delocalized interaction, and on the specific value of the cutoff is mild. We also compare the use of a nonlocal Lagrangian with other approaches investigated in the literature.

The key quantity of the discussion is the propagator of scalar resonances dressed by mesonic loops in one or more channels. When the Källen-Lehmann representation is satisfied, as verified at the one-loop level in the case of light scalar mesons for large ranges of parameters [22], the spectral function (proportional to the imaginary part of the propagator) is correctly normalized and is interpreted as a "mass distribution" for the scalar state. A general definition of the decay of a scalar state, which involves the obtained mass distribution and does not require a study of the properties of the propagator in the complex plane, is then possible. In this way, one takes into account in a consistent fashion finite-width effects for the decay, hence allowing one to study deviations from the usually employed tree-level formula for decay rates. Furthermore, the fulfillment of the Källen-Lehmann representation offers a criterion to delimit the validity of our one-loop study: as soon as violations appear (generally for large coupling constants) the obtained spectral functions are no longer usable.

To render the paper easily understandable and self-contained, we start in Sec. II with the one-channel case by recalling the basic definitions and properties, then we apply the study to the scalar sigma σ and kaon k resonances: the corresponding spectral function shows consistent deviations from the usual Breit-Wigner one. In Sec. III, we turn to the two-channel case, with particular attention to the resonances $a_0(980)$ and $f_0(980)$, their decay rates and spectral functions in comparison with the Flatté distribution [23,24]. Implications of the results in view of a nonet of tetraquark states below 1 GeV is discussed. In Sec. IV, we derive our conclusions, emphasizing as in Ref. [22] that the use of propagators fulfilling the Källen-Lehmann representation, which implies normalized distributions and a correct definition of decay rates, should be preferable both in theoretical and experimental work.

II. SCALAR SPECTRAL FUNCTION: ONE-CHANNEL CASE

A. Definitions and properties

We consider the scalar fields S and φ described by the Lagrangian

$$\mathcal{L}_S^1 = \frac{1}{2}(\partial_\mu S)^2 - \frac{1}{2}M_0^2 S^2 + \frac{1}{2}(\partial_\mu \varphi)^2 - \frac{1}{2}m^2\varphi^2 + gS\varphi^2 \,. \quad (1)$$

In the limit $g = 0$, the propagator of the field S reads

$$\Delta_S(p) = \frac{1}{p^2 - M_0^2 + i\varepsilon}, \quad g = 0 \,. \quad (2)$$

We intend to study the modification to $\Delta_S(p)$ when $g \neq 0$, which arises by considering the loop diagram of Fig. 1, and how this contribution affects the decay mechanism $S \to \varphi\varphi$. We recall that at the tree level, the decay width reads

$$\Gamma^{\text{t-l}}_{S\varphi\varphi}(M_0) = \frac{p_{S\varphi\varphi}}{8\pi M_0^2}[g_{S\varphi\varphi}]^2\theta(M_0 - 2m),$$
$$p_{S\varphi\varphi} = \sqrt{\frac{M_0^2}{4} - m^2}, \quad g_{S\varphi\varphi} = \sqrt{2}g, \quad (3)$$

where $\theta(x)$ is the step function and the factor $\sqrt{2}$ in the amplitude $g_{S\to\varphi\varphi}$ takes into account that the final state consists of two identical particles. In general, the symbol p_{SAB} is understood to be the expression

$$p_{\text{SAB}} = \frac{1}{2M_S}\sqrt{M_S^4 + \left(M_A^2 - M_B^2\right)^2 - 2\left(M_A^2 + M_B^2\right)M_S^2}\,, \quad (4)$$

i.e., the momentum of the outgoing particle(s).

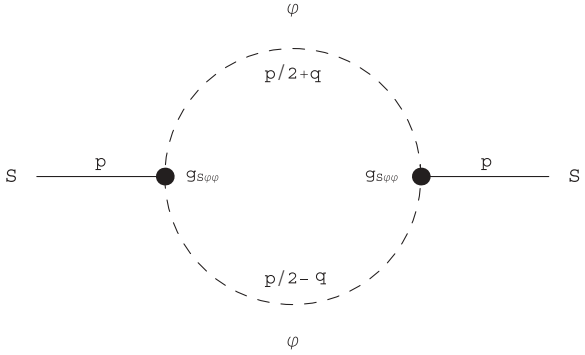

FIG. 1. Mesonic loop.

At tree level, the particle S is treated as stable. However, the very fact that the decay $\Gamma^{\text{t-l}}_{S\varphi\varphi} \neq 0$ for $M_0 > 2m$ means that S is not stable and cannot be considered as an asymptotic state of the Lagrangian $\mathcal{L}_S^1$. The tree-level expression $\Gamma^{\text{t-l}}_{S\varphi\varphi}$ is only valid in the limit $g \to 0$. The evaluation of the loop of Fig. 1 offers a way to define and interpret the decay $S \to \varphi\varphi$ as we describe in the following. The modified propagator of S is obtained by (re)summing the loop diagrams of Fig. 1, that is,

$$\Delta_S(p^2) = \frac{1}{p^2 - M_0^2 + g_{S\varphi\varphi}^2\,\Sigma(p^2) + i\varepsilon}, \quad (5)$$

where the self-energy $\Sigma(p^2)$ reads

$$\Sigma(p^2) = -i\int \frac{d^4q}{(2\pi)^4} \times \frac{1}{[(q+p/2)^2 - m^2 + i\varepsilon][(q-p/2)^2 - m^2 + i\varepsilon]} \,. \quad (6)$$

The integral defining $\Sigma(p^2)$ is, as known, logarithmic divergent. Our intention is to consider the Lagrangian $\mathcal{L}_S^1$ as an effective low-energy description of the fields S and φ, and not as a fundamental theory valid up to indefinitely high mass scales. We do not apply the renormalization scheme to $\mathcal{L}_S^1$, but we introduce a regularization function $f_\Lambda(q)$ which depends on a cutoff scale Λ for the large momenta. The self-energy $\Sigma(p^2)$ is then modified to

$$\Sigma(p^2) = -i\int \frac{d^4q}{(2\pi)^4} \times \frac{f_\Lambda^2(q^o, \vec{q}\,)}{[(q+p/2)^2 - m^2 + i\varepsilon][(q-p/2)^2 - m^2 + i\varepsilon]} \,. \quad (7)$$

When choosing $f_\Lambda(q) = f_\Lambda(q^2)$, the covariance of the theory is preserved, otherwise it is lost. Indeed, in many calculations related to mesonic loops, a regularization of the kind $f_\Lambda(q) = f_\Lambda(\vec{q}^{\,2})$ is chosen, which leads to simple expressions for the self-energy contribution but breaks covariance explicitly, and thus this regularization is strictly valid only in the rest frame of the decaying particle. In particular, the three-dimensional cutoff $f_\Lambda(\vec{q}^{\,2}) = \theta(\Lambda^2 - \vec{q}^{\,2})$ is often used. Appendix A provides a closer analysis of the self-energy $\Sigma(p^2)$ and presents the case of unequal masses circulating in the loop. The interaction strength among light mesons is suppressed for distances larger than $l \sim 0.5$–1 fm: in this particular physical example, it is then natural to implement a cutoff $\Lambda \sim 1/l$, which varies between 1 and 2 GeV.

The cutoff function $f_\Lambda(q)$ is not present in the Lagrangian $\mathcal{L}_S^1$ of Eq. (1). In this sense, the Lagrangian is incomplete because it does not specify how to cut the high momenta. One can take into account $f_\Lambda(q)$ already at the Lagrangian level by

rendering the interaction term nonlocal:

$$\left(\mathcal{L}_S^1\right)_{\rm int} = gS\varphi^2 \to gS\int d^4y\,\varphi\,(x+y/2) \times \varphi\,(x-y/2)\Phi(y)\,. \quad (8)$$

The Feynman rule for the three-leg vertex is modified as

$$ig \to igf_\Lambda\left(\frac{q_1-q_2}{2}\right), \quad f_\Lambda(q) = \int d^4y\,\Phi(y)e^{-iyq}, \quad (9)$$

where q_1 and q_2 are the momenta of the two particles φ. The function $f_\Lambda(q)$ enters directly into the expression of all amplitudes. In particular, the self-energy contribution of Eq. (7) is now obtained by application of the (modified) Feynman rules to the loop diagram of Fig. 1. Indeed, the delocalization of the interaction term also induces a change of the tree-level result for the decay, which becomes [for the case $f_\Lambda(q) = f_\Lambda(\vec{q}^{\,2})$]

$$\Gamma^{\rm t\text{-}l}_{S\varphi\varphi}(M_0) = \frac{p_{S\varphi\varphi}}{8\pi M_0^2}\left[g_{S\varphi\varphi}f_\Lambda\left(\vec{q}^{\,2}=p^2_{S\varphi\varphi}\right)\right]^2\theta(M_0-2m),$$
$$g_{S\varphi\varphi} = \sqrt{2}g, \quad (10)$$

that is, the function $f_\Lambda(\vec{q}^{\,2})$ is explicitly present in the tree-level decay expression and can be interpreted as a phenomenological form factor.[1]

If a step function is used, the local tree-level expression of Eq. (3) is recovered, provided that the cutoff Λ is large enough. In this work, we use the following cutoff function:

$$f_\Lambda(q) = f_\Lambda(\vec{q}^{\,2}) = (1+\vec{q}^{\,2}/\Lambda^2)^{-1}\,. \quad (11)$$

With this choice, the Fourier transform $\Phi(y)$, see Eq. (9), takes the form $\delta(y^0)\exp[-|\vec{y}\,|\Lambda]/|\vec{y}\,|$, thus decreasing rapidly for increasing distance of the two interacting mesons φ. The interaction range l is of the order Λ^{-1}, as discussed above, based on general dimensional grounds. At each step of the forthcoming study, we employed also different forms of $f_\Lambda(q)$, finding that the dependence on the precise form of $f_\Lambda(q)$ affects only slightly the results. Notice that in Ref. [25] a similar equation to Eq. (10) [where $s = \vec{q}^{\,2}$ and $f_\Lambda = G(s)$ in the notation of Ref. [25]] represents the starting point of the analysis. The function $G(s)$ in the above-cited works is taken to be a Gaussian, Λ is of the order of 1 GeV. The present approach shows the link between such a form factor $f_\Lambda = G(s)$ and a nonlocal Lagrangian. However, we do not concentrate as in Ref. [25] on scattering amplitudes but on spectral functions and decay widths. At the same time, we do not relate the imaginary and real parts of the propagator via the Källen-Lehmann dispersion relation, but we evaluate them independently, and subsequently we check numerically if it satisfied, as detailed in the following discussion.

Let us now turn to the self-energy $\Sigma(p^2)$. A general property for $\Sigma(p^2)$ follows from the optical theorem

$$I(x) = g^2_{S\phi\phi}{\rm Im}[\Sigma(x=\sqrt{p^2})] = x\Gamma^{\rm t\text{-}l}_{S\phi\phi}(x)\,. \quad (12)$$

[1]For a covariant vertex function $f_\Lambda(q)$ the decay amplitude takes the form $[g_{S\phi\phi}f_\Lambda(q^0=0,\mathbf{q}^2=p^2_{S\varphi\varphi})]$.

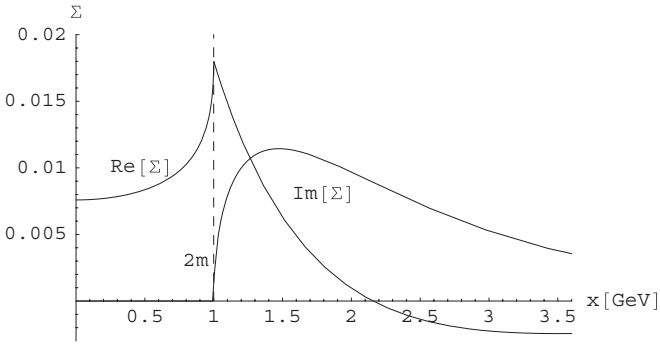

FIG. 2. Real and imaginary parts of the mesonic loop for $m = 0.5$ GeV and $\Lambda = 1.5$ GeV.

The imaginary part of the self-energy diagram is zero for $0 < x < 2m$ and nonzero starting at threshold. The real part

$$R(x) = g^2_{S\varphi\varphi}{\rm Re}[\Sigma(x=\sqrt{p^2})] \quad (13)$$

is nonzero below and above threshold. In Fig. 2 the functions $R(x)$ and $I(x)$ are plotted using Eq. (11). A particular choice is made for the parameters $m = 0.5$ GeV and $\Lambda = 1.5$ GeV (of the order of physical cases studied later). Anyway, the plotted functions are qualitatively similar for large ranges of parameters. As noticeable, $R(x)$ is continuous but not derivable in $x = 2m$. It has a cusp at $x = 2m$: the left derivative is $+\infty$, while the right derivative is finite and negative.

In terms of the two functions $R(x)$ and $I(x)$, the propagator of Eq. (2) reads

$$\Delta_S(x) = \frac{1}{x^2 - M_0^2 + R(x) + iI(x) + i\varepsilon}\,. \quad (14)$$

We define the (Breit-Wigner) mass M for the scalar field S as the solution of the equation

$$M^2 - M_0^2 + R(M) = 0\,. \quad (15)$$

When the function $R(M)$ is positive, which is usually the physical case (Fig. 2), the dressed mass M is smaller than the bare mass M_0, showing that the quantum fluctuations tend to lower it.

We now turn to the spectral function $d_S(x)$ of the scalar field S related to the imaginary part of the propagator as

$$d_S(x) = \frac{2x}{\pi}\left|\lim_{\varepsilon\to 0}{\rm Im}[\Delta_S(x)]\right|. \quad (16)$$

In the limit $g \to 0$, we obtain the desired spectral function $d_S(x) = \delta(x - M_0)$. The normalization of $d_S(x)$ holds for each g, i.e.,

$$\int_0^\infty d_S(x)\,dx = 1\,. \quad (17)$$

The latter equation is a consequence of the Källen-Lehmann representation

$$\Delta_S(x) = \int_0^\infty dy\frac{2y}{\pi}\frac{-{\rm Im}[\Delta_S(y)]}{y^2 - x^2 + i\varepsilon} \quad (18)$$

when taking the limit $x \to \infty$. Equations (17) and (18) hold in general for the full propagator. In our case, we check

numerically the validity of the normalization condition (17) at the one-loop level of Fig. 1. We find that it is fulfilled to a high level of accuracy for large ranges of parameters, see also the discussion in Ref. [22] and in the next section.

Let us consider $d_S(x)$ in the two interesting cases $M < 2m$ and $M > 2m$. If $M < 2m$, Eq. (16) becomes

$$d_S(x) = Z\delta(x - M)\theta(2m - x) + \frac{2x}{\pi}\frac{I(x)}{\left(x^2 - M_0^2 + R(x)\right)^2 + I(x)^2}, \quad (19)$$

where

$$Z = \left[1 + \frac{1}{2M}\left(\frac{dR}{dx}\right)_{x=M}\right]^{-1}. \quad (20)$$

When $M < 2m$, the constant Z is usually reabsorbed into the definition of the wave function renormalization, hence recovering the free propagator properly normalized as $(p^2 - M^2 + i\varepsilon)^{-1}$, corresponding to $d_S(x) = \delta(x - M)$ for $x < 2m$ as in the free case $g = 0$. Thus, we still have a stable particle with dressed mass M instead of M_0. Notice that $0 < Z < 1$ because $R'(M)$ is a positive number: the quantity $(1 - Z)$ can be interpreted as the amount of virtual clouds of 2φ contributing to the wave function.

If $M > 2m$, the spectral function reads

$$d_S(x) = \frac{2x}{\pi}\frac{I(x)}{\left(x^2 - M_0^2 + R(x)\right)^2 + I(x)^2}. \quad (21)$$

No δ functions are present, but typically a picked distribution $d_S(x)$ is obtained, corresponding to a physical resonance. The mass M is not the maximum of the $d_S(x)$, although in general it is very close to it. Consistent deviations can appear when M is close to threshold and for a large coupling constant; see next subsection for a more detailed discussion of this point. Notice moreover that $d_S(x)$ is zero for $x < 2m$.

We plot the typical behavior of the spectral function in both cases $M < 2m$ and $M > 2m$ in Fig. 3. We used the values $M = 0.9$ and $M = 1.3$ GeV corresponding to the the two cases below and above the threshold, $m = 0.5$ GeV as before, and $g_{S\phi\phi} = 3$ GeV. The value of Z, for the subthreshold case, is ∼0.9, and we have numerically verified that the spectral functions are normalized in both cases.

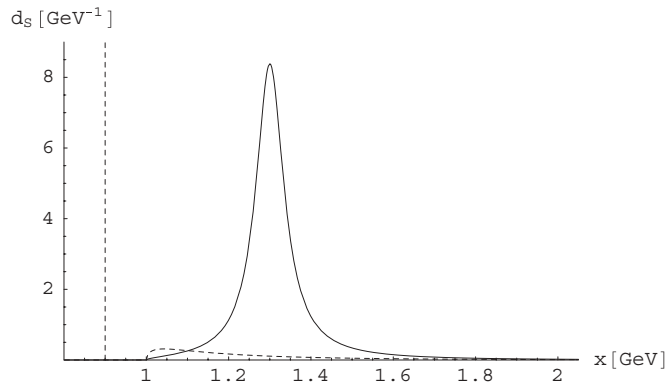

FIG. 3. Spectral functions in the cases $M < 2m$ (dashed line) and $M > 2m$ (continuous line). The coupling constant is $g_{S\phi\phi} = 3$ GeV, the two mass values chosen are $M = 0.9$ and $M = 1.3$ GeV, and $m = 0.5$ GeV.

When $M > 2m$, the function $d_S(x)$ can be interpreted as the mass distribution of the resonance; see also Appendix B for an intuitive discussion about this point. We then define the decay rate for the process $S \to \varphi\varphi$ by implementing the distribution $d_S(x)$, and thus including finite width effects, as

$$\Gamma_{S\varphi\varphi} = \int_0^\infty dx\, d_S(x)\, \Gamma^{\text{t-l}}_{S\varphi\varphi}(x)\,. \quad (22)$$

This formula reduces to the tree-level amplitude $\Gamma^{\text{t-l}}_{S\varphi\varphi}(M_0)$ of Eq. (10) in the limit of small g:

$$\Gamma^{\text{t-l}}_{S\varphi\varphi}(M_0) \simeq \Gamma_{S\varphi\varphi} \quad \text{for } g \to 0\,. \quad (23)$$

Notice that in this limit, $M \to M_0$. However, even for finite g, when $M \neq M_0$, the formula $\Gamma_{S\varphi\varphi} \simeq \Gamma^{\text{t-l}}_{S\varphi\varphi}(M)$ offers a first approximation to the decay width of the state as long as the distribution is picked, i.e., the scalar state S is not too broad. Notice that Eq. (22) does not in general coincide with the standard width obtained by complex analysis search of pole positions, see Ref. [26]. In fact, in our study, only the real valued x variable is considered.

The definition Eq. (22) for the decay $S \to \varphi\varphi$ is thus a generalization of the tree-level result of Eq. (10) and takes automatically into account that the state S has a finite width parametrized by the mass distribution $d_S(x)$, which naturally arises by considering the self-energy of the scalar propagator. Notice that the real part of the propagator is necessary in order for Eq. (17) to hold: its neglect would spoil the correct normalization.

Evaluating the real and imaginary parts at $x = M$ and neglecting their x dependence, the distribution (21) is approximated by

$$d_S^{\text{bw}}(x) \simeq \frac{2M}{\pi}\frac{I(M)}{(x^2 - M^2)^2 + (I(M))^2}, \quad (24)$$

which is the relativistic Breit-Wigner distribution for the resonance S, usually employed in theoretical and experimental studies. However, the distribution $d_S^{\text{bw}}(x)$ neglects the real part of the loop diagram, and consequently the normalization of Eq. (17) does not hold, implying that $d_S^{\text{bw}}(x)$ has to be normalized by hand. At the same time, the mass M does not coincide with the maximum of $d_S(x)$. Thus, we insist on that the usage of automatically normalized distribution emerging from propagators fulfilling Källen-Lehmann should be preferable.

B. Application to the light scalar mesons σ and k

An interesting example for the one-channel case is the decay of the scalar meson $\sigma \equiv f_0(600)$. As reported by the PDG [5], experimental data are affected by large uncertainties both for the value of the mass, $M_\sigma = 0.4$–1.2 GeV, and the value of the Breit-Wigner width, $\Gamma_\sigma = 0.6$–1 GeV. The dominant channel, which we will consider here, is the decay into two pions, for which $M > 2m$.

By applying the formulas of Sec. II A, we show in the left panel of Fig. 4 the spectral functions $d_\sigma(x)$ of the σ resonance

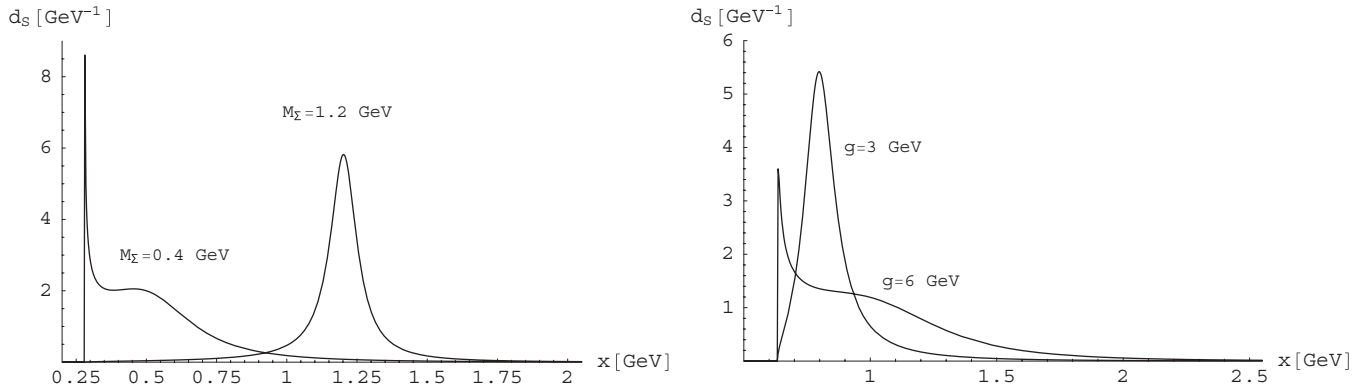

FIG. 4. Spectral functions of σ and k. Left panel: $\Lambda = 1.5$ GeV, $g = 3$ GeV, $M_\sigma = 0.4$ GeV with a correspondent $\Gamma = 0.242$ GeV, and $M_\sigma = 1.2$ GeV with a correspondent $\Gamma = 0.113$ GeV. Right panel: $M_k = 0.8$ GeV, $\Lambda = 1.5$ GeV, $g = 3$ GeV with a correspondent $\Gamma = 0.112$ GeV, and $g = 6$ GeV with a correspondent $\Gamma = 0.382$ GeV.

for the two boundary cases of PDG, namely, $M_\sigma = 0.4$ and $M_\sigma = 1.2$ GeV, for the coupling constant $g_{\sigma\pi\pi} = 3$ GeV.

The spectral function assumes different shapes for different values of the mass. While for $M_\sigma = 1.2$, far from the threshold, the spectral function has a regular Breit-Wigner-like form, in the case $M_\sigma = 0.4$ GeV, a distorted shape, with a narrow peak just above threshold, is visible.[2] The employed value of the coupling constant, $g_{\sigma\pi\pi} = 3$ GeV, serves as illustration and actually corresponds to a somewhat too narrow width. The increase of $g_{\sigma\pi\pi}$ leads, however, outside the range of validity of the normalization of Eq. (17) at the one-loop level; see below.

The description of the scalar kaonic resonance k follows the same line [27]. As shown in the right panel of Fig. 4, a strong deviation from the Breit-Wigner form is obtained when $g_{k\pi K} = 6$ GeV, corresponding to $\Gamma_k = 0.38$ GeV, while a less distorted shape is found for $g_{k\pi K} = 3$ GeV, for which $\Gamma_k = 0.11$ GeV.

At this point, a short discussion on the definition of the mass of an unstable particle is needed. In the Breit-Wigner scheme, the mass of the particle is the value corresponding to the maximum of the spectral function, and it is one parameter of the distribution (the second one is of course the width). In our scheme, using the spectral functions coming from the loop evaluation this is no longer the case: the mass M defined in Eq. (15) is again a parameter of the distribution (together with the coupling constant g), but it does not coincide with the maximum of the distribution. For $M_\sigma = 1.2$ GeV (far from threshold), the maximum of the spectral function occurs at 1.202 GeV, thus only slightly shifted from the mass; however, when $M_\sigma = 0.4$ GeV, the maximum of the spectral function (apart from the threshold enhancement peak) occurs at sizably larger values with respect to the mass, here 0.454 GeV.[3] (Notice also that in the latter case, the bare mass M_0 is 0.614 GeV, thus implying a strong influence of the pion loop to the σ mass, see also Appendix A for a comparison of different "masses".) Indeed, although the mass M being the zero of the real part of the inverse propagator, see Eq. (15), is referred to as a Breit-Wigner mass [25], the best fit to the full spectral function $d_\sigma(x)$ by using a Breit-Wigner form is obtained for a Breit-Wigner mass $M_{\rm BW}$ coinciding with the maximum of the distribution. It is also remarkable that in some cases, the spectral function does not have a maximum, apart from the threshold enhancement peak, as we can see for the k meson in the right panel of Fig. 4 for $g_{k\pi K} = 6$ GeV.

We now study closer the decay process $\sigma \equiv f_0(600) \to \pi\pi$ using Eq. (22) which implements the spectral function $d_\sigma(x)$. In Fig. 5, we compare the full and tree-level decay rates for different values of the cutoff and of the coupling constants (a mass $M_\sigma = 600$ MeV is used).

As expected, there is not a strong dependence on the choice of the cutoff. Moreover, the results obtained with our formulas are well in agreement with the tree-level results for small values of g (since the spectral function tends to a δ function). Nonnegligible differences instead occur for the larger values of g. This is due to a different analytic dependence of the two

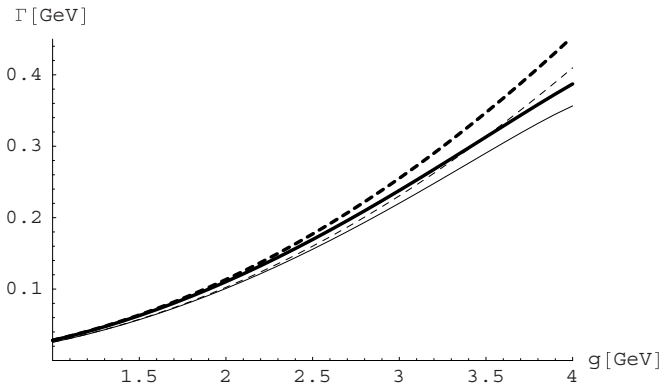

FIG. 5. Full (solid) and tree-level (dashed) decay rates $\sigma \to \pi\pi$ as functions of the coupling constant. The cases $\Lambda = 1$ and $\Lambda = 2$ GeV correspond to thin and thick lines, respectively.

[2] In the limit $M_\sigma \to 2m_\pi$ the spectral function $d_S(x) \sim 1/I(x) \to \infty$ for $x \to 2m_\pi$ due to the threshold enhancement.

[3] Recent theoretical works [18] find a σ mass at around 450 MeV, thus not far from threshold in the lower side of the PDG data. This is indeed the case of an irregular form for the spectral function of this resonance, for which care is needed.

corresponding formulas from the coupling constant: while the tree-level expression depends quadratically on g, in the loop formula g appears also in the distribution $d_S(x)$.

The limit of the validity of the employed one-loop level analysis is an important aspect which deserves further discussion. Namely, when the coupling constant is too large and the mass is not far from threshold, the normalization condition of Eq. (17) is lost; see also the corresponding discussion in Ref. [22]. This fact means that higher orders must be taken into account to satisfy the Källen-Lehmann representation and thus to recover the correct normalization of Eq. (17). At the same time, the violation of the normalization is a valid criterion to establish the limit of our study. For this reason in Fig. 5 we stop the plot at $g_{\sigma\pi\pi} = 4$ GeV (corresponding to $\Gamma_\sigma \sim 400$ MeV); in fact, larger values imply $\int_0^\infty d_S(x)\,dx < 1$. At this point, the full decay width [using Eq. (22)] is already ∼60 MeV smaller than the tree-level counterpart. A decay width of about 400 MeV is on the low side for the σ (see Ref. [21]). In Ref. [18], a width 150 MeV larger is obtained. A study beyond the one-loop level would then be necessary to evaluate the spectral function for larger coupling (i.e., larger width) and represents a possible outlook of the present work. Surely the overestimation of the tree-level formula keeps growing for increasing interaction strengths. Similar considerations hold for the k meson.

III. SCALAR SPECTRAL FUNCTION: TWO-CHANNEL CASE

A. Definitions and properties

We now consider two channels for the scalar resonance S described by the Lagrangian density ($m_2 > m_1$):

$$\mathcal{L}_S^2 = \frac{1}{2}(\partial_\mu S)^2 - \frac{1}{2}M_0^2 S^2 + \frac{1}{2}(\partial_\mu \varphi_1)^2 - \frac{1}{2}m_1^2\varphi_1^2 + \frac{1}{2}(\partial_\mu \varphi_2)^2 - \frac{1}{2}m_2^2\varphi_2^2 + g_1 S\varphi_1^2 + g_2 S\varphi_2^2\,. \quad (25)$$

The processes $S \to \varphi_1\varphi_1$ and $S \to \varphi_2\varphi_2$ correspond to the tree-level decay rates

$$\Gamma^{\text{t-l}}_{S\varphi_1\varphi_1}(M_0) = \frac{p_{S\varphi_1\varphi_1}}{8\pi M_0^2}[g_{S\varphi_1\varphi_1}]^2\theta(M_0 - 2m_1), \qquad g_{S\varphi_1\varphi_1} = \sqrt{2}g_1, \quad (26)$$

$$\Gamma^{\text{t-l}}_{S\varphi_2\varphi_2}(M_0) = \frac{p_{S\varphi_2\varphi_2}}{8\pi M_0^2}[g_{S\varphi_2\varphi_2}]^2\theta(M_0 - 2m_2), \qquad g_{S\varphi_2\varphi_2} = \sqrt{2}g_2\,. \quad (27)$$

The propagator is modified by loops of φ_1 and φ_2, denoted as $\Sigma_1(p^2)$ and $\Sigma_2(p^2)$ and given by Eq. (7) for $m = m_1$ and $m = m_2$, respectively. A delocalization of the interaction, via a vertex function $\Phi(y)$ and the corresponding Fourier transform $f_\Lambda(q) = \int d^4y\,\Phi(y)e^{-iyq}$, is then introduced as in Eq. (8) for both channels in order to regularize the self-energy contributions. As a consequence, the tree-level results are modified as

$$\Gamma^{\text{t-l}}_{S\varphi_1\varphi_1}(M_0) = \frac{p_{S\varphi_1\varphi_1}}{8\pi M_0^2}\left[g_{S\varphi_1\varphi_1} f_\Lambda\left(\overrightarrow{q}^{\,2} = p^2_{S\varphi_1\varphi_1}\right)\right]^2 \times \theta(M_0 - 2m_1), \quad (28)$$

$$\Gamma^{\text{t-l}}_{S\varphi_2\varphi_2}(M_0) = \frac{p_{S\varphi_2\varphi_2}}{8\pi M_0^2}\left[g_{S\varphi_2\varphi_2} f_\Lambda\left(\overrightarrow{q}^{\,2} = p^2_{S\varphi_2\varphi_2}\right)\right]^2 \times \theta(M_0 - 2m_2), \quad (29)$$

and the propagator as

$$\Delta_S(x) = \frac{1}{x^2 - M_0^2 + R(x) + iI(x) + i\varepsilon}\,. \quad (30)$$

where

$$R(x) = g^2_{S\varphi_1\varphi_1}\mathrm{Re}[\Sigma_1(x = \sqrt{p^2})] + g^2_{S\varphi_2\varphi_2}\mathrm{Re}[\Sigma_2(x = \sqrt{p^2})], \quad (31)$$

and

$$I(x) = g^2_{S\varphi_1\varphi_1}\mathrm{Im}[\Sigma_1(x = \sqrt{p^2})] + g^2_{S\varphi_2\varphi_2}\mathrm{Im}[\Sigma_2(x = \sqrt{p^2})] \quad (32)$$

$$= x\Gamma^{\text{t-l}}_{S\varphi_1\varphi_1}(x) + x\Gamma^{\text{t-l}}_{S\varphi_2\varphi_2}(x)\,. \quad (33)$$

In the last equation, the optical theorem was used. The mass M of the state S is given by $M^2 - M_0^2 + R(M) = 0$. Again, we have two cases:

(i) $M < 2m_1$: the distribution $d_S(x)$ takes the form $Z\delta(x - M)$ for $x < 2m_1$. The discussion is similar to the one-channel case; Eq. (19) is still valid. At threshold $2m_1$, the continuum starts.

(ii) $M > 2m_1$: as in Eq. (21), the distribution is

$$d_S(x) = \frac{2x}{\pi}\frac{I(x)}{\left(x^2 - M_0^2 + R(x)\right)^2 + I(x)^2}\,. \quad (34)$$

It vanishes for $M < 2m_1$. At $x = 2m_2$, the second channel opens.

In case (ii), we have a resonant state. The decay rates into the two channels $S \to \varphi_1\varphi_1$ and $S \to \varphi_2\varphi_2$ are given by the integrals

$$\Gamma_{S\varphi_1\varphi_1} = \int_0^\infty dx\, d_S(x)\,\Gamma^{\text{t-l}}_{S\varphi_1\varphi_1}(x), \qquad \Gamma_{S\varphi_2\varphi_2} = \int_0^\infty dx\, d_S(x)\,\Gamma^{\text{t-l}}_{S\varphi_2\varphi_2}(x). \quad (35)$$

A particularly interesting case takes place when $2m_1 < M < 2m_2$. While the tree-level result for $S \to \varphi_2\varphi_2$ vanishes, we find that $\Gamma_{S\varphi_2\varphi_2}$ is not zero. In this case, the tree-level approximation is absolutely not applicable: the particle S does decay in virtue of the high-mass tail of its distribution. A physical example is well known: the resonances $f_0(980)$ and $a_0(980)$ have a nonzero decay rate into $\overline{K}K$, although their masses are below the threshold $2m_K$. Clearly, a sizable decay rate $\Gamma_{S\varphi_2\varphi_2}$ is obtained only when M is close to threshold. A generalization to the present definitions to N channels is straightforward [22].

When applying the decay formulas (36) it is, however, important to verify numerically that the normalization of the distribution $d_S(x)$ holds; in fact, as discussed in Sec. II B, the formalism is self-consistent in this case.

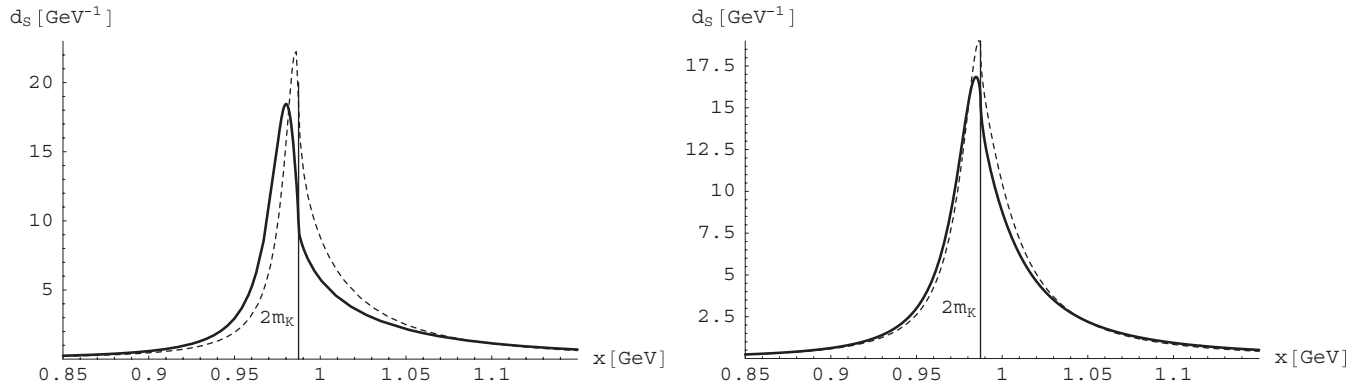

FIG. 6. Left panel: spectral function of f_0 within our formalism (solid line) and using the Flatté distribution (dashed line). Parameters are: $\Lambda = 1.5$ GeV, $g_{f_0 K\overline{K}} = 3$ GeV with a correspondent total decay rate $\Gamma = 0.058$ GeV. Right panel: same as left panel, but for spectral function of a_0, and $\Gamma = 0.048$ GeV.

B. Application to $a_0(980)$ and $f_0(980)$

In this section, we study the spectral functions of the scalar mesons $a_0 \equiv a_0(980)$ and $f_0 \equiv f_0(980)$, whose masses are $M_{a_0} = 984.7 \pm 1.2$ MeV and $M_{f_0} = 980 \pm 10$ MeV [5]. For both resonances, two decays have been observed: $a_0 \to \pi\eta$, $a_0 \to K\overline{K}$ and $f_0 \to \pi\pi$, $f_0 \to K\overline{K}$. Notice that both masses are below the threshold of kaon-antikaon production, $M_{a_0, f_0} < 2M_K = 987.3$ MeV, thus the decay of both resonances in $K\overline{K}$ vanishes at tree-level, while experimentally it was seen for both a_0 and f_0 states.

For definiteness, we use the ratios obtained in the experimental analysis [4], i.e.,

$$\frac{g^2_{f_0 K\overline{K}}}{g^2_{f_0\pi\pi}} = 4.21 \pm 0.46, \qquad \frac{g^2_{f_0 K\overline{K}}}{g^2_{a_0 K\overline{K}}} = 2.15 \pm 0.40,$$
$$\frac{g^2_{a_0\pi\eta}}{g^2_{a_0 K\overline{K}}} = 0.75 \pm 0.11, \tag{36}$$

thereby leaving us with only one free parameter, chosen to be $g_{f_0 K\overline{K}}$. Although experimental uncertainties are still large, the results of Eq. (36) are qualitatively similar to those of various studies, see Ref. [24] and references therein, pointing to a large $K\overline{K}$ coupling for both resonances with a particular enhancement for f_0 (see Refs. [4,10,11,15] and references therein for spectroscopic interpretations).

For the typical value $g_{f_0 K\overline{K}} = 3$ GeV, we report in Fig. 6 the spectral functions of a_0 and f_0. There is a large probability, $\sim$50%, in both cases, that these two mesons have a mass larger than the threshold of production $2m_K$, and therefore the tree-level forbidden decay occurs. In the same figure, we compare our distribution with the Flatté one [23,24], which is usually employed for the a_0 and f_0 mesons. At variance from our distribution, the Flatté distribution must be normalized by hand. The two distributions are quite similar, except that for f_0 the values of the mass corresponding to the maximum of the distributions are slightly different. This is due to the strong coupling of f_0 to kaons, and, as already argued by Achasov [22], the meson loop distributions coincide with the Flatté ones only in the limit of weak coupling.

In Fig. 7, we show the decay rates $f_0 \to \pi\pi$, $f_0 \to K\overline{K}$ and $a_0 \to \pi\eta$, $a_0 \to K\overline{K}$ as function of $g_{f_0 K\overline{K}}$. The dashed areas in both plots correspond to the total decay rate of f_0 and a_0 as indicated by the PDG (notice, however, that

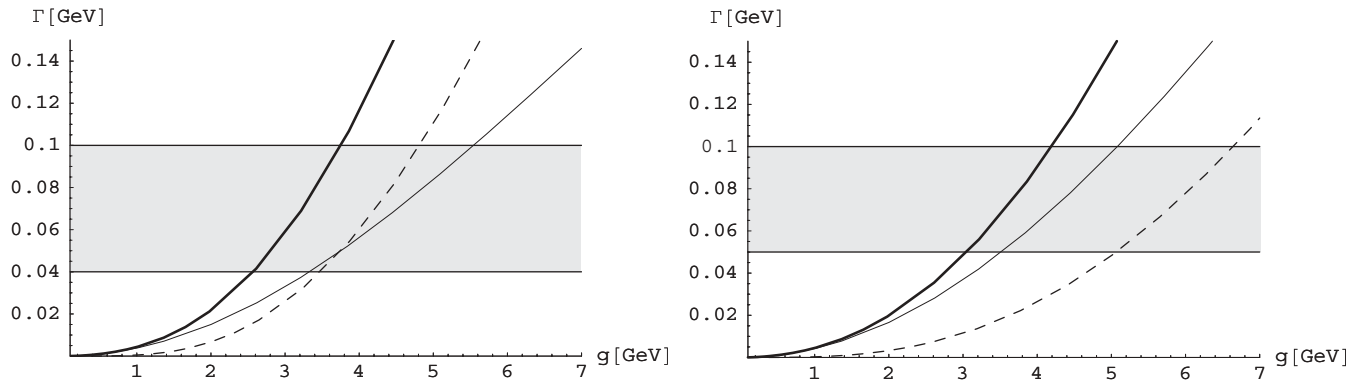

FIG. 7. Left panel: decay rates of f_0 as functions of the coupling constant g. The thin solid line corresponds to the decay into two pions, the dashed line to the decay into two kaons, and the thick solid line is the sum of the two decay rates. Right panel: decay rates of a_0 as functions of the coupling constant g. The thin solid line corresponds to the decay into pion and η, the dashed line to the decay into two kaons, and the thick solid line is the sum of the two decay rates.

PDG specified that the real width could be larger). For our theoretical total decay rates to agree with the measured ones, $g_{f_0 K\overline{K}}$ has to lie between 3 and 4 GeV. The outcoming branching ratio $\Gamma_{a_0 K\overline{K}}/\Gamma_{a_0\pi\eta}$ is ∼0.3–0.4, which is larger than the PDG average of 0.183 ± 0.024; while the obtained ratio $\Gamma_{f_0\pi\pi}/(\Gamma_{f_0\pi\pi} + \Gamma_{f_0 K\overline{K}})$ is ∼0.48–0.56, which is in qualitative agreement with the (not bold) results listed by the PDG. Notice furthermore that the f_0 meson typically has a larger width than the a_0 meson, in agreement with Ref. [24].

We finally comment on a possible tetraquark unified interpretation of the light scalar mesons as presented in Ref. [11]. A too small decay constant $g_{f_0 K\overline{K}}$ would also imply by far too narrow σ and k mesons (related by Clebsh-Gordon coefficients [11]), thus against a tetraquark nonet. On the contrary, $g_{f_0 K\overline{K}}$ between 3 and 4 GeV is in agreement with a tetraquark nonet below 1 GeV, although problems, such as a too narrow k, persist, see discussions in [11,15]. Such a strong coupling in the $K\overline{K}$ channel implies that a virtual cloud of kaon-antikaon pairs plays an important role, in particular for the f_0 resonance. A heuristic indicator of the mesonic cloud can be given by the quantity

$$Z_{\overline{K}K} = \left[1 + \frac{1}{2M_S}\left(\frac{dR_{\overline{S}KK}}{dx}\right)_{x=M_S}\right]^{-1},$$

where $R_{S\overline{K}K} = g^2_{S\overline{K}K}\mathrm{Re}[\Sigma_{KK}(x)]$ (with $S = f_0, a_0$) refers to the kaonic loop only. As discussed in Sec. II, in the subthreshold case (which applies to the kaonic channel here) the quantity $(1 - Z)$ varies between 0 and 1 and measures the mesonic cloud dressing of the original bare resonance S. In the f_0 case, by using Eq. (36) together with $g_{f_0 K\overline{K}} = 3$ GeV, one finds $(1 - Z_{\overline{K}K}) = 0.38$, hence implying a 38% of kaonic cloud. This number increases for increasing coupling strength $g_{f_0 K\overline{K}}$. This discussion confirms the interpretation put forward in Ref. [2], where the light scalar mesons possess a tetraquark core but are dressed by kaonic clouds. We also refer the reader to Ref. [28] for a related study of the a_0 and f_0 mesons that employs the so-called compositeness condition introduced by Weinberg in Ref. [29].

IV. SUMMARY AND CONCLUSIONS

In this work we studied the spectral functions of scalar mesons in one- and two-channel cases suitable for the description of light scalar mesons below 1 GeV. We have computed, by using nonlocal interaction Lagrangians with nonderivative couplings, the propagators of scalar mesons at the one-loop level. They satisfy for large ranges of parameters the Källen-Lehmann representation, therefore implying normalized spectral functions. In this way a correct definition of decay amplitudes, weighted over the spectral function, is formulated: the finite-width effects are automatically taken into account. The resulting decay rates are smaller than the tree-level ones with increasing mismatch for increasing interaction strength. On the other hand, a subthreshold tree-level forbidden decay, such as the $K\overline{K}$ mode for $a_0(980)$ and $f_0(980)$, becomes large.

The resulting spectral functions for the σ and k mesons may deviate consistently from the Breit-Wigner form. The Flatté distribution, although it approximates to a good level of accuracy the $a_0(980)$ and $f_0(980)$ spectral functions, emerges as a small-coupling limit of our more general spectral function.

As stressed by Achasov [22], it is important to use distributions satisfying Källen-Lehmann representations in experimental and theoretical studies. We thus believe that the use of distributions obtained from quantum field theoretical models fulfilling the correct normalization requirements can be helpful in correctly disentangling the nature of the scalar states. Future studies with derivative couplings, mixing effects, such as in the recent work of Ref. [30], and ϕ decays represent a possible interesting outlook.

ACKNOWLEDGMENTS

G.P. acknowledges financial support from INFN.

APPENDIX A: LOOP CONTRIBUTIONS

Here we report basic formulas for the loop diagram of Eq. (7) drawn in Fig. 1 for the vertex function $f_\Lambda(q) = f_\Lambda(\overrightarrow{q}^2)$. By evaluating the residua, one obtains the one-dimensional integral

$$\Sigma(x^2 = p^2) = \frac{1}{2\pi^2}\int_0^\infty dw \frac{w^2 f_\Lambda^2(w)}{\sqrt{w^2 + m^2}(4(w^2 + m^2) - x^2)}, \tag{A1}$$

which can be easily evaluated numerically for each well-behaved $f_\Lambda(w)$. We recall that within our conventions $f_\Lambda(0) = 1$ and that $w = |\overrightarrow{k}|$; Eq. (A1) refers to a three-dimensional vertex function. In Ref. [22], the form $f_\Lambda(w) = \theta(\Lambda - w)$ is used and the limit $\Lambda \to \infty$ is taken. As described in the text, we did not follow this procedure; instead, we used a definite form(s) for the vertex function $f_\Lambda(w)$. As remarked in the text, we performed the calculations also with different forms for $f_\Lambda(w)$ (different power form and exponential functions): the precise form of the cutoff function does not affect the physical picture.

When the scalar state S couples to two particles of masses m_1 and m_2, the loop contribution is modified as

$$\Sigma(x) = \frac{1}{4\pi^2}\int_0^\infty dw \frac{w^2\left(\sqrt{w^2 + m_1^2} + \sqrt{w^2 + m_2^2}\right) f_\Lambda^2(w)}{\sqrt{w^2 + m_1^2}\sqrt{w^2 + m_2^2}\left[\left(\sqrt{w^2 + m_1^2} + \sqrt{w^2 + m_2^2}\right)^2 - x^2\right]}. \tag{A2}$$

TABLE I. Comparison of masses.

M	M_0	$M_{\max}$	$\langle M\rangle$
0.4	0.61	0.45	0.54
0.6	0.71	0.62	0.65
0.8	0.86	0.81	0.82
1	1.03	1.00	1.01

The choice $f_\Lambda(w) = (1 + w^2/\Lambda^2)^{-1}$ with $\Lambda = 1$–2 GeV has been used in this work.

In relation to the mass definition of Sec. II B, we report and compare in Table I the mass M defined in Eq. (15), the bare mass M_0, the maximum $M_{\max}$ of the distribution $d_{S\equiv\sigma}(x)$, and the average mass $\langle M\rangle = \int_0^\infty dx\, x\, d_S(x)$. We use $m = m_\pi$, $g_{\sigma\pi\pi} = 3$ GeV, and $\Lambda = 1.5$ GeV.

As expected, the larger the mass, the smaller the differences among the various masslike quantities.

APPENDIX B: SPECTRAL FUNCTION AS MASS DISTRIBUTION: AN INTUITIVE DISCUSSION

We present an intuitive argument for the correctness of interpretation of the spectral function $d_S(x)$ as the "mass distribution" of the state S. To this end, we introduce two scalar fields A and B, the first massless and the second with $M_B > M_S$, and write down the interaction Lagrangian

$$L = cBAS + gS\varphi^2. \tag{B1}$$

[for the following discussion, the "delocalization" of Eq. (8) is not important]. We suppose that the interaction strength c is small enough to allow a tree-level analysis for the decay of the state B. The term $cBAS$ generates the decay process $B \to AS$, which reads (at tree-level)

$$\Gamma^{\text{t-l}}_{BAS}(M_B) = \frac{p_{BAS}}{8\pi M_B^2}[c]^2. \tag{B2}$$

However, when $g \neq 0$ the state S decays into $\varphi\varphi$; that is, the state S is not an asymptotic state. Physically, we observe a tree-body decay $B \to A\varphi\varphi$, whose decay-rate reads

$$\Gamma^{\text{t-l}}_{BA\varphi\varphi}(M_B) = \int_0^{M_B} \Gamma^{\text{t-l}}_{BAS}(M_B)\, d_S(x)\, dx. \tag{B3}$$

The tree-body decay is decomposed into two steps: $B \to AS$ and $S \to \varphi\varphi$. The quantity $\Gamma^{\text{t-l}}_{BAS}(M_B)$ represents the probability for $B \to AS$ (at a given mass x for the state S) and $d_S(x)\, dx$ is the corresponding weight, i.e., the probability that the resonance S has a mass between x and $x + dx$. In this example, $d_S(x)$ emerges naturally as a mass distribution, correctly normalized, for the scalar state S. Furthermore, notice that in virtue of the limit $d_S(x) = \delta(M - M_S)$ for $g \to 0$, one has

$$\Gamma^{\text{t-l}}_{BA\varphi\varphi}(M_B) = \Gamma^{\text{t-l}}_{BAS}(M_B) \quad \text{for } g \to 0. \tag{B4}$$

In fact, if g is very small, the state S is long lived and Eq. (B2) is recovered. The present analysis also shows that studies on the tree-body decay of the ϕ meson can be consistent only if propagators satisfying the Källen-Lehmann representation are used.

[1] C. Amsler and N. A. Tornqvist, Phys. Rep. **389**, 61 (2004).
[2] F. E. Close and N. A. Tornqvist, J. Phys. G **28**, R249 (2002).
[3] R. L. Jaffe, Phys. Rep. **409**, 1 (2005) [Nucl. Phys. Proc. Suppl. **142**, 343 (2005)]; R. L. Jaffe, arXiv:hep-ph/0701038; M. R. Pennington, arXiv:hep-ph/0703256; N. N. Achasov, arXiv:hep-ph/0609261.
[4] D. V. Bugg, Eur. Phys. J. C **47**, 57 (2006); D. V. Bugg, *ibid.* **47**, 45 (2006).
[5] W. M. Yao *et al.* (Particle Data Group), J. Phys. G **33**, 1 (2006).
[6] C. Amsler and F. E. Close, Phys. Lett. **B353**, 385 (1995); C. Amsler and F. E. Close, Phys. Rev. D **53**, 295 (1996).
[7] R. L. Jaffe, Phys. Rev. D **15**, 267 (1977); R. L. Jaffe, *ibid.* **15**, 281 (1977); R. L. Jaffe and F. E. Low, *ibid.* **19**, 2105 (1979).
[8] M. B. Voloshin and L. B. Okun, JETP Lett. **23**, 333 (1976) [Pis'ma Zh. Eksp. Teor. Fiz. **23**, 369 (1976)]; K. Maltman and N. Isgur, Phys. Rev. Lett. **50**, 1827 (1983); K. Maltman and N. Isgur, Phys. Rev. D **29**, 952 (1984).
[9] L. Maiani, F. Piccinini, A. D. Polosa, and V. Riquer, Phys. Rev. Lett. **93**, 212002 (2004).
[10] N. N. Achasov and V. N. Ivanchenko, Nucl. Phys. **B315**, 465 (1989); N. N. Achasov and V. V. Gubin, Phys. Rev. D **64**, 094016 (2001).
[11] F. Giacosa, Phys. Rev. D **74**, 014028 (2006) .
[12] F. E. Close and A. Kirk, Eur. Phys. J. C **21**, 531 (2001); W. J. Lee and D. Weingarten, Phys. Rev. D **61**, 014015 (1999); M. Strohmeier-Presicek, T. Gutsche, R. Vinh Mau, and A. Faessler, *ibid.* **60**, 054010 (1999);F. Giacosa, T. Gutsche, and A. Faessler, Phys. Rev. C **71**, 025202 (2005); F. Giacosa, T. Gutsche, V. E. Lyubovitskij, and A. Faessler, Phys. Rev. D **72**, 094006 (2005); F. Giacosa, T. Gutsche, V. E. Lyubovitskij, and A. Faessler, Phys. Lett. **B622**, 277 (2005); G. Mosconi (private communication).
[13] D. Black, A. H. Fariborz, S. Moussa, S. Nasri, and J. Schechter, Phys. Rev. D **64**, 014031 (2001).
[14] A. H. Fariborz, R. Jora, and J. Schechter, Phys. Rev. D **72**, 034001 (2005); A. H. Fariborz, Int. J. Mod. Phys. A **19**, 2095 (2004); A. H. Fariborz, Phys. Rev. D **74**, 054030 (2006); M. Napsuciale and S. Rodriguez, *ibid.* **70**, 094043 (2004).
[15] F. Giacosa, Phys. Rev. D **75**, 054007 (2007).
[16] E. van Beveren, F. Kleefeld, G. Rupp, and M. D. Scadron, Mod. Phys. Lett. A **17**, 1673 (2002); M. D. Scadron, G. Rupp, F. Kleefeld, and E. van Beveren, Phys. Rev. D **69**, 014010 (2004); **69**, 059901(E) (2004).
[17] P. Minkowski and W. Ochs, Nucl. Phys. B Proc. Suppl. **121**, 123 (2003).
[18] I. Caprini, G. Colangelo, and H. Leutwyler, Phys. Rev. Lett. **96**, 132001 (2006); G. Colangelo, J. Gasser, and H. Leutwyler, Nucl. Phys. **B603**, 125 (2001).
[19] J. A. Oller, E. Oset, and J. R. Pelaez, Phys. Rev. D **59**, 074001 (1999); **60**, 099906(E) (1999)].
[20] J. R. Pelaez, Phys. Rev. Lett. **92**, 102001 (2004); Mod. Phys. Lett. **A19**, 2879 (2004); J. R. Pelaez and G. Rios, Phys. Rev. Lett. **97**, 242002 (2006).

[21] M. Ishida, Prog. Theor. Phys. **101**, 661 (1999); Z. H. Guo, L. Y. Xiao, and H. Q. Zheng, arXiv:hep-ph/0610434.
[22] N. N. Achasov and A. V. Kiselev, Phys. Rev. D **70**, 111901(R) (2004).
[23] S. M. Flatté, Phys. Lett. **B63**, 228 (1976).
[24] V. Baru, J. Haidenbauer, C. Hanhart, A. Kudryavtsev, and U. G. Meissner, Eur. Phys. J. A **23**, 523 (2005).
[25] N. A. Tornqvist, Z. Phys. C **68**, 647 (1995); M. Boglione and M. R. Pennington, Phys. Rev. D **65**, 114010 (2002).
[26] R. Escribano, A. Gallegos, J. L. Lucio, M. G. Moreno, and J. Pestieau, Eur. Phys. J. C **28**, 107 (2003); T. Bhattacharya and S. Willenbrock, Phys. Rev. D **47**, 4022 (1993).
[27] The resonance $k(800)$ is now listed in the compilation of the Particle Data Group [5] but it still needs confirmation and is omitted from the summary table. The resonance is also found in many recent theoretical and experimental works (Refs. [4,19], E. Van Beveren, T. A. Rijken, K. Metzger, C. Dullemond, G. Rupp, and J. E. Ribeiro, Z. Phys. C **30**, 615 (1986); S. Ishida, M. Ishida, T. Ishida, K. Takamatsu, and T. Tsuru, Prog. Theor. Phys. **98**, 621 (1997); D. Black, A. H. Fariborz, F. Sannino, and J. Schechter, Phys. Rev. D **58**, 054012 (1998) and references therein.)
[28] V. Baru, J. Haidenbauer, C. Hanhart, Yu. Kalashnikova, and A. E. Kudryavtsev, Phys. Lett. **B586**, 53 (2004); B. Kerbikov, *ibid*. **B596**, 200 (2004) .
[29] S. Weinberg, Phys. Rev. **130**, 776 (1963).
[30] C. Hanhart, B. Kubis, and J. R. Pelaez, Phys. Rev. D **76**, 074028 (2007).